Local Controller for an Autonomous Grid-Supportive Battery Energy Storage System

Roshan Sharma*, Student Member, IEEE, Ali Zakerian, Student Member, IEEE, Masoud Karimi-Ghartemani, Senior Member, IEEE,

Abstract—This paper presents the complete design of a local controller for a grid-supportive battery energy storage (BES) system. The controller's objectives are 1) to execute commands issued from the secondary controller, 2) to provide grid support, 3) to prevent converter over-current during transient low-voltage incidents, and 4) to maintain the state-of-charge (SOC) of the battery. The grid support is divided into static, i.e. the droopbased, and dynamic, i.e. the inertia-based, voltage supports. The proposed controller uses an optimally designed full-state feedback approach which merges the voltage and current controllers. This makes the design more systematic, flexible, and with better tradeoff in speed and damping. The proposed BES is autonomous meaning that it does not have to be co-located with a renewable resource. This autonomous feature allows the BES to connect to any critical node in a system, detect disturbances through local measurements, and provide support regardless of the origin of the disturbance. Mathematical derivations, computer simulations, and laboratory experimental results of the proposed controller are presented in this paper.

Index Terms—Battery energy storage (BES) system, intermittence of renewable sources, grid support, capacitor emulation, virtual inertia, dc microgrid

I. INTRODUCTION

ENEWABLE energy resources, such as solar photo-Notaic (PV) and wind energy, are being increasingly deployed in modern power system due to the technological advancements, increasing public awareness, and governmental supports. The levelized cost of energy (LCOE) of residential, commercial, and utility scale PVs are 10¢, 8¢, and 6¢ per kWh, respectively in 2020—down from 52¢, 40¢, and 28¢ in 2010-and are expected to go down another 50% by 2030 [1]. The installation of PV is expanding with a global projection of 13% annually from 2020 to 2030, contributing to almost one-third of electricity demand [2]. However, the uncertain and intermittent nature of PV still constitutes a major challenge against its high penetration. The abrupt disturbances cause voltage fluctuations, over-voltage or under-voltage situations, and even instabilities [3]–[5]. Standards are increasingly stipulate complying indices for distributed energy resources (DERs). According to IEEE Standard 1547, a DER cannot cause voltage fluctuations exceeding 3% for a medium voltage and 5% for a low voltage interconnection [6]. The battery energy storage (BES) technologies are considered as means for balancing the intermittence. They are expected to play a major

The authors are with the Department of Electrical and Computer Engineering, Mississippi State University, E-mail addresses: rs2142@msstate.edu, az364@msstate.edu, and karimi@ece.msstate.edu.

* Corresponding author

role in the emerging power grid. They may even serve as the anchoring sources at high penetration of renewable sources. The cost of battery technology has also decreased over recent years. For example, the price of the lithium-ion battery has also decreased from \$1100/kWh in 2010 to \$156/kWh in 2019, and projected to reduce to \$61/kWh by 2030 [7].

Microgrid, a cluster of DERs and loads with a single point of coupling to the main grid, is a promising way of control and coordination of a large number of DERs. With the proliferation of PV and BES technologies, the dc and hybrid dc/ac energy systems are increasingly used [8]–[11] to reduce the number and size of conversion systems, and reduce the power conversion losses. The dc distribution is advantageous in applications involving electric vehicle (EV) charging, data centers, telecommunication towers, LEDs, and household devices [12]–[14].

To address the PV disturbances, a number of solutions have been presented. In [15], the PV curtails the generation in case of over-voltage at the cost of total revenues. In [16], when the PV power suddenly rises, it is curtailed and a ramp rate control is applied. This method cannot address the ramping down of the PV. Ramping or filtering the PV power using battery and capacitors is proposed in [17]-[20]. In [17], moving average based control is proposed using electric double-layer capacitor to respond to PV fluctuations exceeding a certain limit. In [18], a BES station is used for PV/wind power smoothing. The power levels of the BES units are adjusted based on the fluctuations and the state-of-charge (SOC) levels. Direct ramp rate control of the PV power is presented in [19]. The methods in [18], [19] do not present how the dynamics of the converter are addressed in the control design. The method in [20] presents the details of the control design to ramp the PV power at the desired rate during disturbances. However, the BES controllers in [17]-[20] require real-time measurement of PV output, which strict the location of the storage device and need a high-speed communication link. Moreover, the BES responds to the disturbances that originate from its local PV only. A centralized power management strategy based on virtual inertia is presented in [21]. It also requires a high-speed communication link between the converters.

The synchronous generators (SGs) have formed a largely stable power grid thanks to their powerful inertial and governor responses. Therefore, virtual synchronous machines have been proposed to mimic the SGs in the ac systems [22]–[24]. The analogous concept has been extended for dc and hybrid dc/ac systems [25], [26]. In [27], a controller for three-phase inverter is proposed that provides virtual inertia to the dc side by

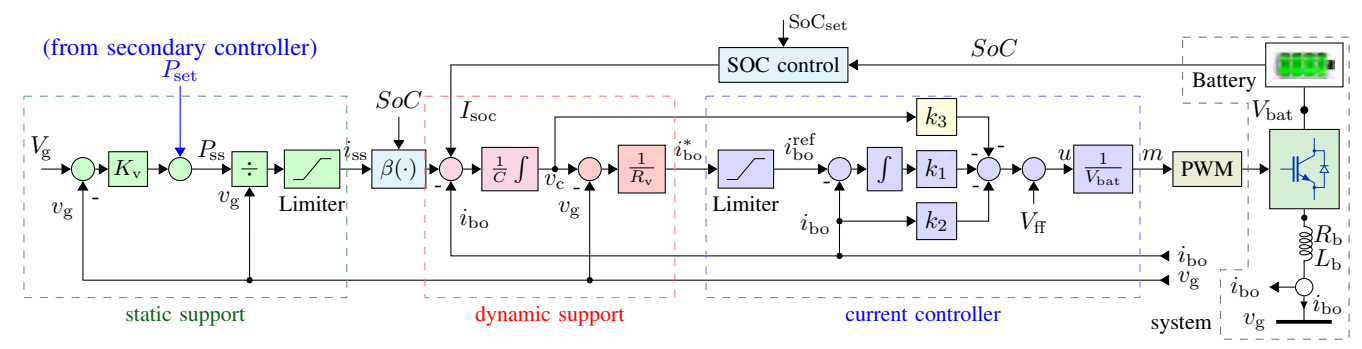


Fig. 1: Block diagram presentation of the proposed dc grid-supportive controller.

adjusting the voltage of the dc link capacitors. However, this method is not applicable for converters with BES because of fixed voltages. The droop gain is adjusted in [28] to generate extra power during the voltage fluctuations. This method, however, introduces voltage differentiation into the control strategy that may excite high-frequency dynamics. SOC based virtual inertia is introduced in [29] that adjusts the droop gain based on the SOC of the BES. A capacitor emulation approach is presented in [30]–[32] to provide inertia during system disturbances. The controllers in [29]–[32] have cascaded proportional integrating (PI) based voltage and current controllers whose performance deteriorates due to interaction of current and voltage loop, especially during weak grid situations.

In this paper, we propose a controller for a grid-supportive BES system to address the multiple issues discussed above. The proposed controller uses the idea of capacitor emulation and droop control to provide dynamic and static supports. Unlike the common practice of separately designing the current and voltage loops, the proposed controller uses an optimally designed full-state feedback controller where the voltage loop is merged in the current loop. This provides more flexibility in design with robust performance. More particularly, the proposed controller simultaneously addresses the following aspects. 1) It is autonomous and is not dependent on a local renewable resource. This allows the BES to connect to any critical node, detect the disturbances through local measurement without requiring high-speed communication, and provide support during the disturbances regardless of their origin. 2) It can execute commands from a central controller. These commands are determined by the central controller considering the economic and technical aspects of the system and coordination with other resources for optimal power/energy management. 3) Both dynamic (or inertia) and static (or droop) supports are provided and their levels are easily adjustable. 4) It allows optimal full-state feedback control design leading to more robust responses. 5) It prevents the over-current of the BES converter against transient low-voltage incidents. 6) An SOC controller is incorporated.

II. PROPOSED CONTROLLER AND SYSTEM EQUATIONS

Figure 1 shows the block diagram of the system, including a battery connected to a dc bus via a bi-directional converter and its proposed controller. The dc bus, denoted by the voltage

 $v_{\rm g}$, can be a node in a dc grid/microgrid or the dc-link of a dc/dc or dc/ac converter depending on the application.

The system disturbances leave a signature on the dc bus voltage v_g . The BES detects this signature and responds accordingly. This response has two grid support components: 1) Dynamic support is an inertia-type response generated by emulation of a capacitor with capacitance C, and 2) Static support is a droop-type response generated by the term $K_v(V_g - v_g)$, where V_g is the nominal value of v_g . The controller also limits the converter current to protect it against transient low-voltage disturbances and maintains the SOC of the battery.

For a bi-directional full-bridge voltage source converter (VSC), if m(t) is the modulating signal of the PWM and $V_{\rm bat}$ is the battery voltage, the average output voltage of the converter is $v_{\rm bo}(t) = m(t)V_{\rm bat}$. Define $u(t) = m(t)V_{\rm bat}$ as the control input, then

$$\frac{\dot{d}}{dt}i_{bo}(t) = -\frac{R_{b}}{L_{b}}i_{bo}(t) + \frac{1}{L_{b}}u(t) - \frac{1}{L_{b}}v_{g}(t)$$
 (1)

where $i_{\rm bo}(t)$ is the output current of the converter, $L_{\rm b}$ is the inductance of the filter, and $R_{\rm b}$ is its parasitic resistance. The mathematical model of the entire proposed BES system and controller is shown in Fig. 2 (a) which is derived based on averaging of signals over a switching cycle.

The dynamic grid support is achieved using capacitor emulation as shown by "capacitor emulation" in Fig 2. (a). This establishes the relation

$$I^* - i_{\text{bo}} = C\dot{v}_{\text{c}} \tag{2}$$

where $I^* = i_{\rm ss} + I_{\rm soc}$ is supplied by the slower external loops. This follows the dynamics of a virtual capacitor with capacitance C and voltage $v_{\rm c}$ as shown in Fig. 2 (b).

In order to provide a support to the grid voltage, the grid voltage v_g and the capacitor voltage v_c must be coupled. This is done by the "voltage loop". The "voltage loop" establishes

$$v_{\rm c} - v_{\rm g} = i_{\rm bo}^* R_{\rm v} \tag{3}$$

where $R_{\rm v}$ is a positive constant. Since the current control loop is fast, the converter output current $i_{\rm bo}$ is equal to $i_{\rm bo}^*$ at the timescale of the voltage loop. Thus, (3) indicates a virtual resistance $R_{\rm v}$ between the virtual capacitor and the dc voltage as shown in Fig. 2 (c). Therefore, the "capacitor emulation" and "voltage loop" together emulate the capacitor C connected to the dc bus through the resistor $R_{\rm v}$. Conventionally, a PI controller is commonly used for this block, which complicates

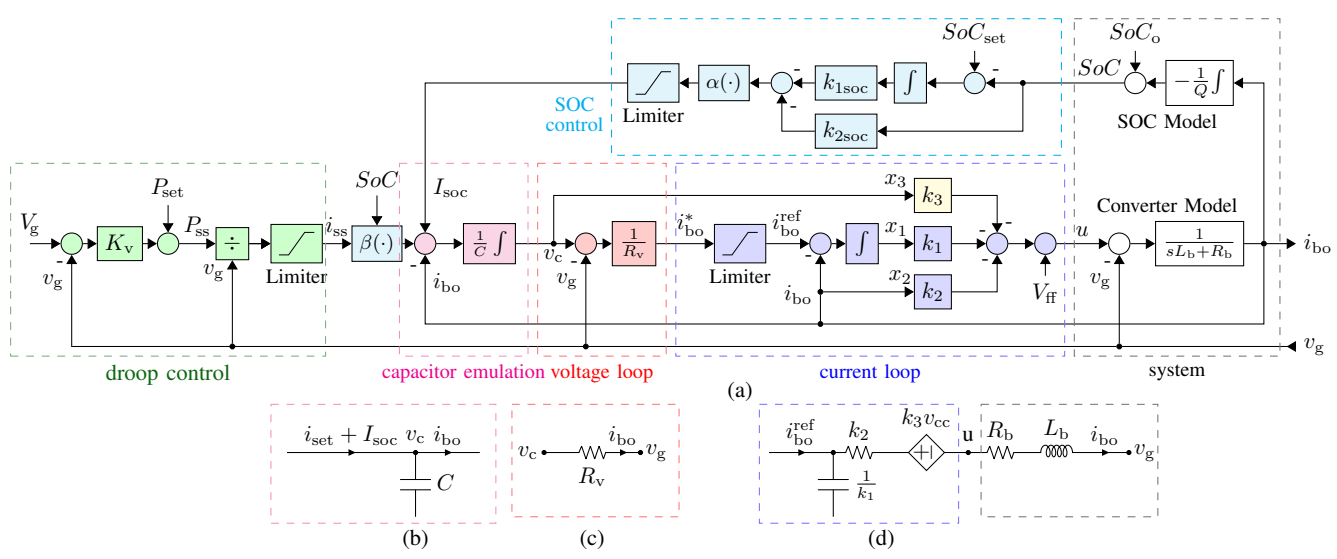


Fig. 2: a) Mathematical model of the proposed BES system, b) Equivalent circuit of capacitor emulation, c) Equivalent circuit of voltage loop (between v_c and v_g), and d) Equivalent circuit of fast current loop.

the design and can also compromise the stability margins of the controller as shown in Section IV-B6.

The static support is expressed by droop function as

$$P_{\rm ss} = P_{\rm set} + K_{\rm v}(V_{\rm g} - v_{\rm g}) \tag{4}$$

where $P_{\rm set}$ is the power set-point, and $K_{\rm v}$ is the droop gain. Current control loop is the innermost loop in Fig. 2(a). It must be fast to tightly regulate the converter current, $i_{\rm bo}$, at the reference value, $i_{\rm bo}^{\rm ref}$. Contrary to the existing literature which do not use a feedback of v_c in this control loop, a full-state feedback with the gains k_1 , k_2 , and k_3 is used in this paper to achieve full control.

The SOC of a battery is the ratio of available charge capacity to its total value. Mathematically, it can be expressed as

$$SoC(t) = SoC_{o} - \frac{1}{Q} \int_{0}^{t} i_{bo}(t)dt \Rightarrow \frac{d}{dt} SoC(t) = -\frac{1}{Q} i_{bo}(t) \quad (5)$$

where $SoC_{\rm o}$ is the initial SOC, and Q is the charge capacity in Ampere-second. The SOC controller generates the increment current, $I_{\rm soc}$, to drive the SOC to its set-point $SoC_{\rm set}$. The parameter α adjusts the strength of SOC control, and β adjusts the level of static support based on the SOC status.

Remark 1: The central controller can communicate low-bandwidth power commands to the BES system, shown by $P_{\rm set}$ in Figs. 1 and 2. This set-point is obtained at the secondary level by solving a given optimization problem considering the economic dispatch of the available resources for optimal power/energy management. The optimization at secondary level control is beyond the scope of this paper. The locally generated static and dynamic supports are added on the top of this power command. The central controller can also optimize $SOC_{\rm set}$, as well as the level of static and dynamic supports determined by $K_{\rm v}$ and C, respectively.

III. DESIGN OF PROPOSED CONTROLLER

The proposed controller has the following 10 parameters: C, R_v , K_v , the current control gains k_1, k_2, k_3 , the SOC control gains $(k_{1\text{soc}}, k_{2\text{soc}})$ and the SOC-driven parameters (α, β) . Their design is explained in this section.

1) Virtual Capacitor (C): The capacitor generates the inertia (or dynamic) power

$$P_{\rm dyn} = -Cv_{\rm c}\dot{v}_{\rm c} \approx -Cv_{g}\dot{v}_{g} \approx -CV_{g}\dot{v}_{g}. \tag{6}$$

The system voltage V_g , its rate of fluctuations \dot{v}_g , and the desired level of support will lead to a proper choice of C.

- 2) Virtual Resistor $(R_{\rm v})$: For an "actual" capacitor directly connected to the dc bus, the voltage of the capacitor is equal to the voltage of the dc system, i.e. the resistance is zero. Here, we have to consider a non-zero $R_{\rm v}$ to allow the controller function properly. The resulted RC circuit has a cut-off frequency of $f_{\rm c}=\frac{1}{2\pi R_{\rm v}C}$. Therefore, $R_{\rm v}$ should be small enough to allow a sufficiently large bandwidth. However, too small $R_{\rm v}$ increases sensitivity to the noises and the sharp jumps in $v_{\rm g}$ and results in over-modulation. The recommended value of $R_{\rm v}$ is between 0.01 p.u. to 0.1 p.u.
- 3) Droop Gain (K_v) : It is set $K_v = \frac{P_{\rm rated}}{\Delta V_{\rm g}}$ where $P_{\rm rated}$ is the rated power of the BES and $\Delta V_{\rm g}$ is the allowable voltage deviation at dc bus. The output of this module is passed through a limiter for extreme voltage transient conditions.
- 4) Current Control Gains (k_1, k_2, k_3) : The design is done using the linear quadratic tracker (LQT) technique. In Fig. 2 (a), assume $x_1(t) = \int e(t)dt = \int (-i_{\mathrm{bo}}(t) + i_{\mathrm{bo}}^{\mathrm{ref}}(t))dt$, $x_2(t) = i_{\mathrm{bo}}(t)$, and $x_3(t) = v_{\mathrm{c}}(t)$. Thus,

$$\dot{x}_{1} = -x_{2} + \frac{x_{3}}{R_{v}} - \frac{v_{g}}{R_{v}}, \ \dot{x}_{2} = -\frac{R_{b}}{L_{b}}x_{2} + \frac{u}{L_{b}} - \frac{v_{g}}{L_{b}}$$

$$\dot{x}_{3} = -\frac{x_{2}}{C} + \frac{i_{ss} + I_{soc}}{C}, \ u = -k_{1}x_{1} - k_{2}x_{2} - k_{3}x_{3} + V_{ff}$$
(7)

where the constant feed-forward term $V_{\rm ff} = v_{\rm g}(0) + k_3 v_{\rm c}(0)$ is for the soft start. The term $v_{\rm g}(0)$ may be replaced with a filtered version of the grid voltage for improved current limiting. The objective is that x_2 tracks its reference in the presence of disturbance. This is a robust tracking problem which can be converted to a linear quadratic regulator (LQR)

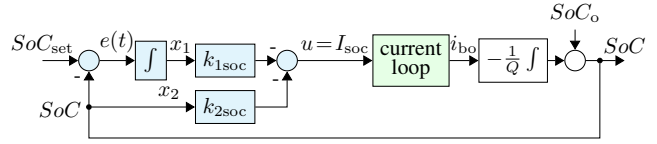


Fig. 3: SOC control loop.

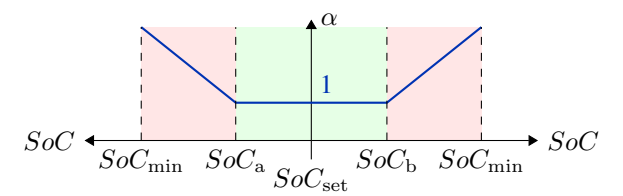


Fig. 4: Adjusting α on varying SoC.

problem by applying $\frac{d}{dt}$ to both sides of (7) to obtain

$$\dot{z}_1 = -z_2 + \frac{1}{R_{\rm v}} z_3, \ \dot{z}_2 = -\frac{R_{\rm b}}{L_{\rm b}} z_2 + \frac{1}{L_{\rm b}} w
\dot{z}_3 = -\frac{1}{C} z_2, \ w = -k_1 z_1 - k_2 z_2 - k_3 z_3$$
(8)

where $z_{\rm i}(t)=\dot{x}_{\rm i}(t)$, and $w(t)=\dot{u}(t)$. The current command components $i_{\rm ss}$ and $I_{\rm soc}$ have slow dynamics and the grid voltage, $v_{\rm g}$, is a dc quantity. Therefore, $\frac{d}{dt}v_{\rm g}=\frac{d}{dt}i_{\rm ss}=\frac{d}{dt}I_{\rm soc}=0$. The equation set (8) is

$$\dot{z}(t) = Az(t) + Bw(t), \quad w(t) = -Kz(t) \tag{9}$$

where

$$A = \begin{bmatrix} 0 & -1 & \frac{1}{R_{v}} \\ 0 & -\frac{R_{b}}{L_{b}} & 0 \\ 0 & -\frac{1}{C} & 0 \end{bmatrix}, B = \begin{bmatrix} 0 \\ \frac{1}{L_{b}} \\ 0 \end{bmatrix}, K = \begin{bmatrix} k_{1} \\ k_{2} \\ k_{3} \end{bmatrix}^{T}.$$

The objective is to regulate $z_1(t) = e(t)$ at 0. Define a cost

$$J = \int_0^\infty \left[q_1 e^2(t) + q_2 z_2^2(t) + q_3 z_3^2(t) + w^2(t) \right] dt. \quad (10)$$

The parameters q_i 's can be systematically adjusted for the design of K to achieve fast and smooth response in current control [33]. The numerical designs are shown in Section IV. Remark 2: In the conventional structure, Fig. 21, the current and voltage loops are nested and designed separately (branch k_3 is absent). This means the voltage loop should be made several times slower than the current loop. However, forcing the current loop to have a very high bandwidth to allow a larger bandwidth margin in the voltage loop may lead to over-modulation of PWM during the transients. The proposed controller does not suffer from this issue. With an extra feedback branch k_3 , consideration of virtual capacitance (C) and virtual resistance (R_v), both loops are merged. This makes the choice of R_v more flexible to obtain sufficient speed and damping in the proposed controller.

Remark 3: For the soft start, the integrator in the 'capacitor emulation' is initialized at $v_{\rm g}(0)$. Moreover, during the current limiting mode, the voltage of the virtual capacitor is frozen to achieve a smooth limiting and transition to normal condition.

5) SOC Control Gains ($k_{1\text{soc}}$, $k_{2\text{soc}}$): They are designed using the approach in [20], [34]. Since this loop is slow, the dynamic support and current control loop are considered as unity during the design as shown in Fig 3. Let $x_1(t) = \int (-SoC(t) + SoC_{\text{set}}) dt$, $x_2(t) = SoC(t)$, and $u(t) = I_{\text{soc}}(t)$.

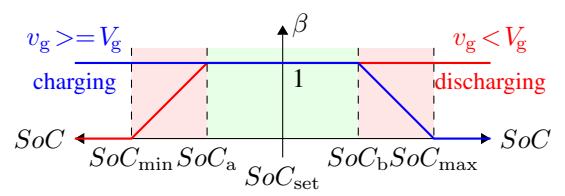


Fig. 5: Adjusting β on varying SoC.

The state equations are

$$\dot{x}_1 = -x_2 + SoC_{\text{set}}, \ \dot{x}_2 = -\frac{1}{Q}u, \ u = -k_{1\text{soc}}x_1 - k_{2\text{soc}}x_2$$
 (11)

The objective is that x_2 tracks its reference in the presence of disturbances. This is converted into an LQR problem by applying $\frac{d}{dt}$ to both sides of (11) to obtain

$$\dot{z}_1 = -z_2, \ \dot{z}_2 = -\frac{1}{Q}w, \ w = -k_{1\text{soc}}z_1 - k_{2\text{soc}}z_2$$
 (12)

where $z_i = \dot{x}_i$ and $w = \dot{u}$. The equation set (12) is

$$\dot{z}(t) = Az(t) + Bw(t), \quad w(t) = -Kz(t)$$
 (13)

where

$$A = \begin{bmatrix} 0 & -1 \\ 0 & 0 \end{bmatrix}, \ B = \begin{bmatrix} 0 \\ -\frac{1}{Q} \end{bmatrix}, \ K = \begin{bmatrix} k_{1 \text{soc}} \\ k_{2 \text{soc}} \end{bmatrix}.$$

The objective is to regulate $z_1 = e(t)$ to 0. Define the cost

$$J = \int_0^\infty [q_1 e^2(t) + q_2 z_2^2(t) + w^2(t)] dt, \tag{14}$$

where q_i 's can be systematically adjusted to design K [33].

6) SOC Control Rate (α) : It adjusts the rate of charge/discharge. It is set as

$$\alpha = \begin{cases} 1, & \text{for } SoC_{\text{a}} < SoC < SoC_{\text{b}} \\ 1 + \gamma |SoC - SoC_{\text{set}}|, & \text{otherwise} \end{cases}$$
 (15)

where γ is a positive constant, Fig. 4. This works by increasing the strength of the SOC controller as the actual value of SOC distances from the desired value.

7) Static Support Adjust Gain (β): This adjusts the static support term as SoC distances from its set-point and prevents possible depletion or overcharging [35]. The design is shown in Fig. 5 which is expressed as

$$\beta = \begin{cases} 1, & \text{if } v_{\rm g} < V_{\rm g} \text{ AND } SoC_{\rm a} \leq SoC \\ \frac{SoC - SoC_{\min}}{SoC_{\rm a} - SoC_{\min}}, & \text{if } v_{\rm g} < V_{\rm g} \text{ AND } SoC_{\min} < SoC < SoC_{\rm a} \\ 0, & \text{if } v_{\rm g} < V_{\rm g} \text{ AND } SoC \leq SoC_{\min} \end{cases}$$

$$1, & \text{if } v_{\rm g} \geq V_{\rm g} \text{ AND } SoC \leq SoC_{\rm b}$$

$$\frac{SoC_{\max} - SoC}{SoC_{\max} - SoC_{\rm b}}, & \text{if } v_{\rm g} \geq V_{\rm g} \text{ AND } SoC_{\rm b} < SoC < SoC_{\max} \\ 0, & \text{if } v_{\rm g} \geq V_{\rm g} \text{ AND } SoC_{\max} \leq SoC \end{cases}$$

$$0, & \text{if } v_{\rm g} \geq V_{\rm g} \text{ AND } SoC_{\max} \leq SoC$$

$$(16)$$

where SoC_{\min} and SoC_{\max} are minimum and maximum limits. The controller starts reducing the static support when the SoC crosses the lower/upper boundaries, $SoC_{\rm a}$ and $SoC_{\rm b}$.

IV. NUMERICAL DESIGNS AND SIMULATION RESULTS

A. System and Parameters

Figure 6 shows the study system. It has a 14-bus dc system consisting of a PV system of 15 kW at bus-7, the proposed BES at bus-8, and the loads at different nodes. The loads are of three types- constant resistance (R-type), constant power (P-type), and constant current (I-type). The nominal dc voltage of the system is 400 V. The dc line parameters and the loads

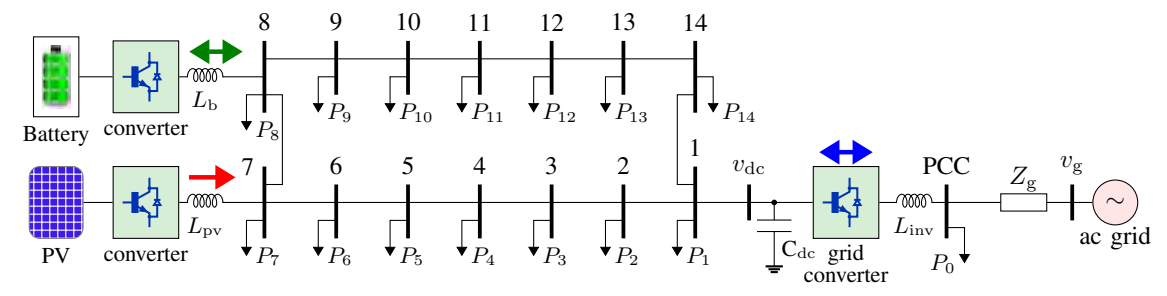


Fig. 6: Study system: an dc/ac hybrid system including a dc microgid (PV, BES, and loads) connected to an ac system.

TABLE I: Parameters of the dc microgrid of the study system

Dc lines						Dc loads		
$r = 0.642 \Omega/\text{km}, \;\; l = 0.22016 \text{ mH/km}$						Bus	Type	(kW)
Line		Length	R	L		1	R	1.00
From	To	(km)	(Ω)	(mH)		2	R	1.20
1	$v_{ m dc}$	1.00	0.6420	0.220		3	I	1.25
1	2	0.50	0.3210	0.110		4	I	0.40
2	3	0.25	0.1605	0.055		5	P	1.75
3	4	2.00	1.2840	0.440		6	R	1.50
4	5	0.75	0.4815	0.165		7	P	0.90
5	6	0.80	0.5136	0.176		8	R	0.45
6	7	0.30	0.1926	0.066		9	R	0.80
7	8	0.50	0.3210	0.110		10	I	2.50
8	9	1.5	0.9630	0.330		11	P	0.60
9	10	1.40	0.8988	0.308		12	R	1.80
10	11	0.20	0.1284	0.044		13	R	0.35
11	12	0.50	0.3120	0.110		14	I	0.50
12	13	0.60	0.3852	0.132		Total		15.00
13	14	0.40	0.2568	0.088				
14	1	2.25	1.4445	0.495				

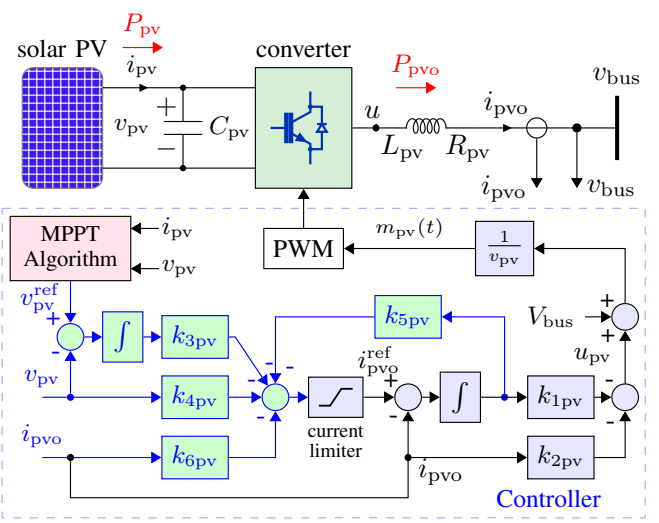


Fig. 7: PV system and its control.

are shown in Table I. The dc system is connected to an ac system via a three-phase converter of 18 kVA. The ac system is modeled as a three-phase ac source behind a grid impedance of $Z_{\rm g}=0.1194+j1.194~\Omega$. The nominal ac voltage at the point of common coupling is 208 V (L-L) and a local ac load (P_0) of 7.07 kVA (at 0.7 PF lagging) is connected. The switching frequency of each converter is 10 kHz. More details on the components of the system are given below.

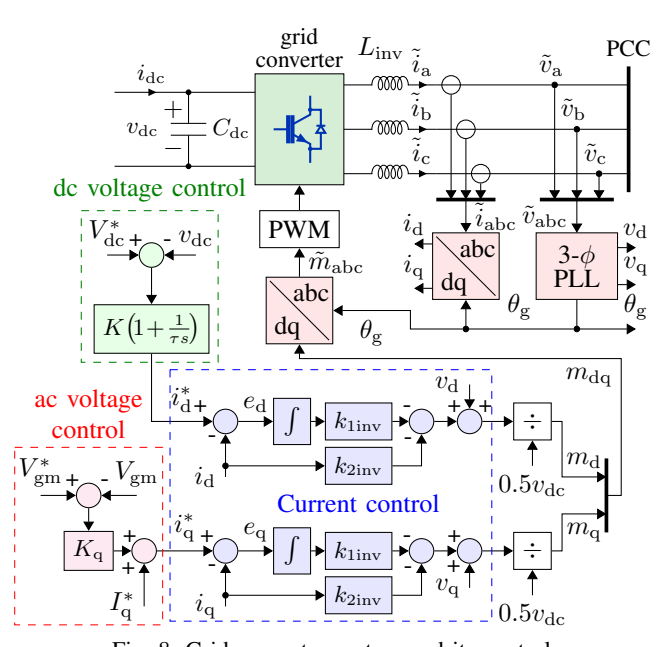


Fig. 8: Grid converter system and its control.

- 1) PV System: The 15 kW PV converter consists of dc-link capacitor of $C_{\rm pv}=500~\mu{\rm F},$ and the output filter $L_{\rm pv}=2.5~{\rm mH},~R_{\rm pv}=50~{\rm m}\Omega,$ Fig. 7. The control structure and design is from [20], [36] leading to $k_{\rm 1pv}=-1333.35,~k_{\rm 2pv}=2.82,$ and $k_{\rm 3pv}=237.13,~k_{\rm 4pv}=-1.14,~k_{\rm 5pv}=829.43,~k_{\rm 6pv}=0.59.$ A perturb and observe MPPT algorithm [37] is used.
- 2) Grid Converter: A three-phase VSC with the standard dq frame current control approach is used as shown in Fig. 8. The dc link capacitance is $C_{\rm dc}=1.2$ mF and the filter is 2.5 mH with 50 m Ω . The VSC regulates the dc voltage at $V_{\rm dc}^*=400$ V using a PI controller (K=-0.2848, $\tau=1/75$). The VSC also provides volt/var support using droop mechanism ($K_{\rm q}\!=\!-0.0577$, $I_{\rm q}^*\!=\!-7.84$ A). The current control gains ($k_{\rm 1inv}\!=\!-1000$, $k_{\rm 2inv}\!=\!2.26$) are designed using the optimal control. The decoupling terms are disabled for improved robustness against weak grid conditions [38]. A three-phase synchronous reference frame (SRF) phase-locked loop (PLL), [39, Chapter 6], with the parameters ($\mu_1=\mu_3=200$, $\mu_2=5000$), is used in the simulation studies.
- 3) Battery System: A 600 V, 10 kW battery equipped with the proposed controller is connected at bus-8 of the dc microgrid via a full-bridge VSC. The rated current of the BES converter is 25 A. The converter consists of an output filter of $L_{\rm b}=2.5~{\rm mH}$ and $R_{\rm b}=50~{\rm m}\Omega$. Unipolar PWM is used.

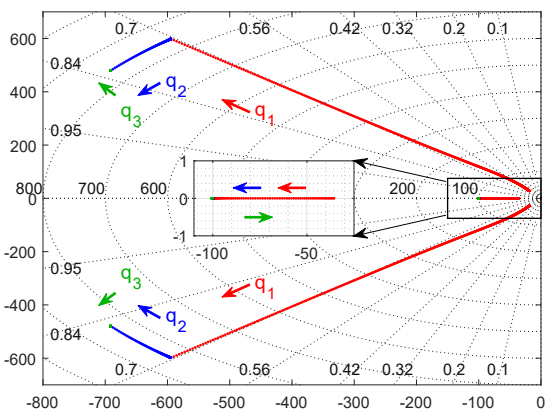


Fig. 9: Design of current controller gains of BES converter.

The converter current is limited within $I_{\rm min}=-40$ A and $I_{\rm max}\!=\!40$ A.

The emulated capacitance is C=100 mF. The virtual resistance $R_{\rm v}=0.10$ gives the bandwidth of the RC circuit around 16 Hz which is sufficient. The current control gains are designed based on the method discussed in Section III-4. Figure 9 shows the plot of the closed loop poles when q_1 , q_2 , and q_3 are subsequently increased between $10^0 \rightarrow 10^{6.5}$, $10^{-2} \rightarrow 10^{0.5}$, and $10^1 \rightarrow 10^2$, respectively. The closed loop poles are at -100 and $-692 \pm j480$ with the control gains $k_1=-1778.28$, $k_2=3.66$, and $k_3=-34.10$. For the static support, the BES supplies its rated power of 10 kW when the dc voltage deviates 20 V (i.e. 5%). Therefore, $K_{\rm v}=500$.

B. Simulation Results

1) Dynamic Support Tests: First, the static support is disabled i.e. $K_{\rm v}=0$, and only the inertial property of the proposed control is studied. To have a point of reference, the performance is compared with an actual capacitor.

Figure 10 shows the response to step jumps in PV power at $t=0.5\ s$ and $t=1.25\ s$. Without a compensator, the voltages across the entire nodes experience fluctuations and offsets. The voltage at the battery terminals (bus-8), and at both dc and ac sides of the grid converter are also shown. The proposed BES has been able to function like an actual capacitor and suppress the voltage fluctuations.

Figure 11 shows the response when a load of 4.0 kW is connected to bus-9 at $t=0.5\ s$ and disconnected at $t=1.5\ s$. Without compensation, the load change causes sharp voltage fluctuations. The proposed BES controller removes the voltage fluctuations just like an actual capacitor.

2) Full Support Tests: The static support is enabled by setting droop gain $K_{\rm v}=500$. Figure 12 shows the system responses to abrupt PV power changes at t=0.5~s and t=1.25~s. The responses of Dynamic Support alone and Full Support (Dynamic+Static) are shown for comparison. With the static support feature enabled, the BES continues to supply power when the voltage settles below 400 V and absorbs power when the voltage settles above 400 V. As a result, the voltage is confined within much narrower bounds. Notice that since the grid converter controls the dc voltage at the point of common coupling (PCC) anyway, the static support does not have much impact on this particular node.

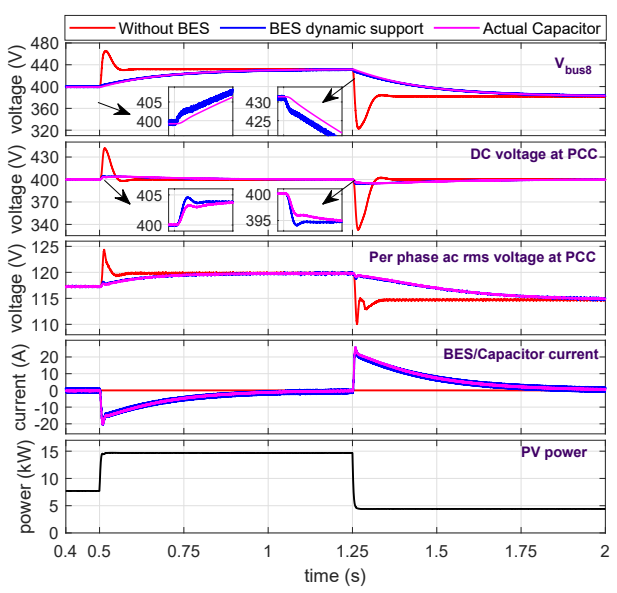


Fig. 10: Dynamic support test 1: Impact of BES system to suppress voltage fluctuations caused by abrupt PV power variations.

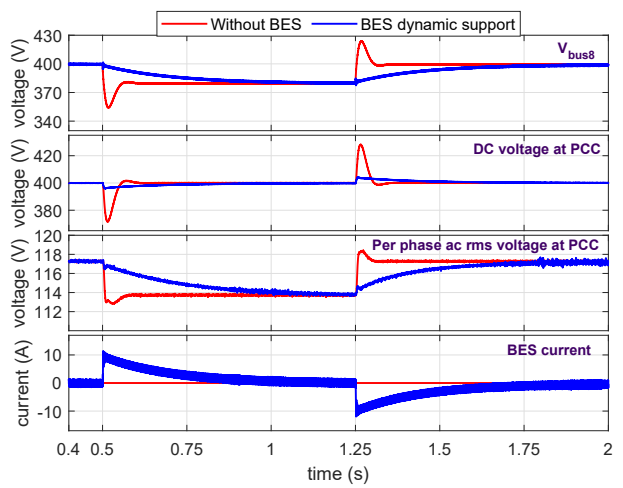


Fig. 11: Dynamic support test 2: Impact of BES system to suppress voltage fluctuations caused by abrupt load changes.

Figure 13 shows the system responses when the load of 4.0 kW is connected/disconnected at $t=0.5 \ s/t=1.25 \ s$. With the static support, the BES provides steady-state support and keeps the voltage within a narrower band.

The grid converter current during PV power fluctuations and load variations are shown in Figs. 14 and 15, respectively. The dynamic support of the BES acts as a buffer to the abrupt stress on the grid converter. With the static support enabled, the grid converter has less stress in its steady operation during the power disturbances.

3) Current Limiting Test: Figure 16 shows the current limiting feature of the proposed controller during severe voltage transients. At $t=0.5\ s$, the voltage of dc bus-8 falls to 10 V and it is restored to normal at $t=0.6\ s$. This deep voltage drop demands a large amount of current from the BES system. The BES, however, successfully limits its current at 40 A to protect the converter. Similarly, at $t=0.75\ s$, there is a voltage rise to 550 V and the dc bus voltage drops back to normal at $t=0.85\ s$. During this voltage rise, the BES absorbs large

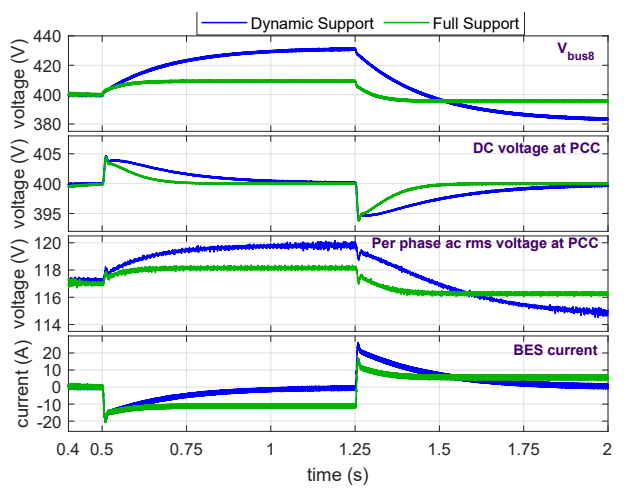


Fig. 12: Full support test 1: Impact of BES to lower voltage fluctuations (dynamic) and offsets (static) caused by PV power variations.

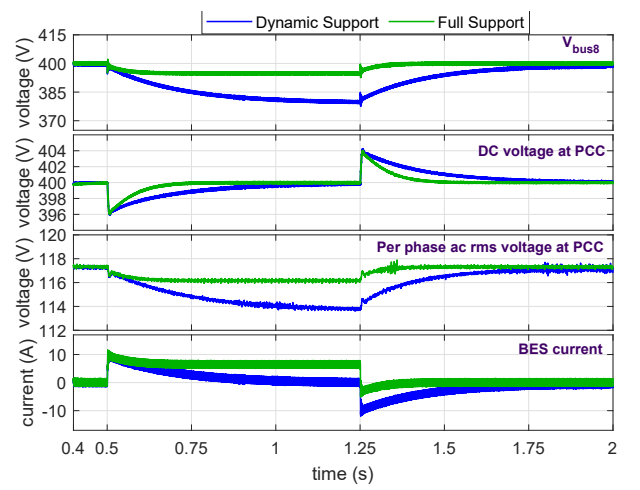


Fig. 13: Full support test 2: Impact of BES to lower voltage fluctuations (dynamic) and offsets (static) caused by load variations.

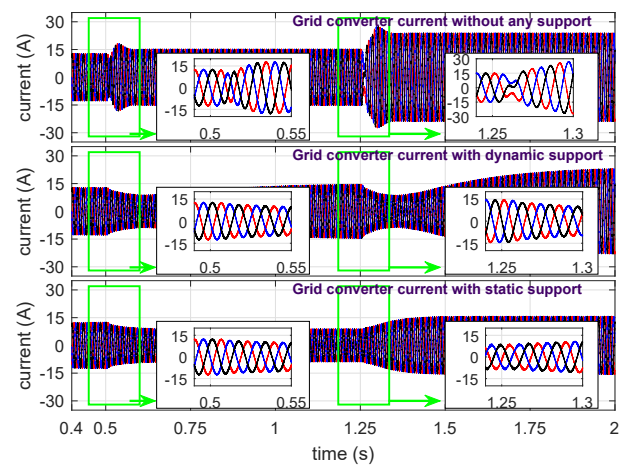


Fig. 14: Grid converter current during PV power fluctuations.

amount of current from the system to help reduce the voltage. The converter current is successfully limited at -40 A.

4) ac Fault Test: Figure 17 shows the responses of the system during a single line-to-ground fault at 1/2 of the grid impedance $Z_{\rm g}$. The fault occurs at t=0.4~s and clears at t=0.5~s. Without BES, the entire system experiences voltage

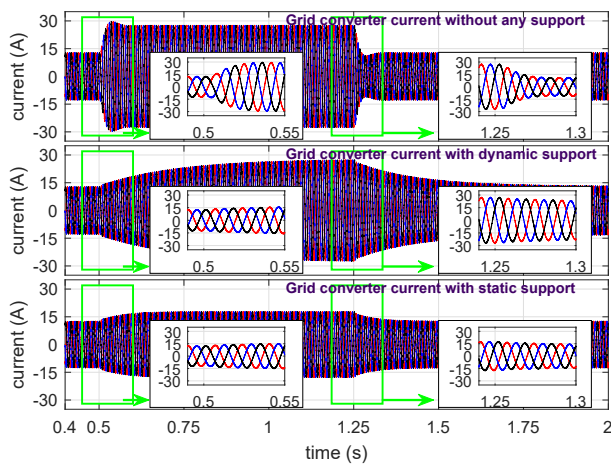


Fig. 15: Grid converter current during load variations.

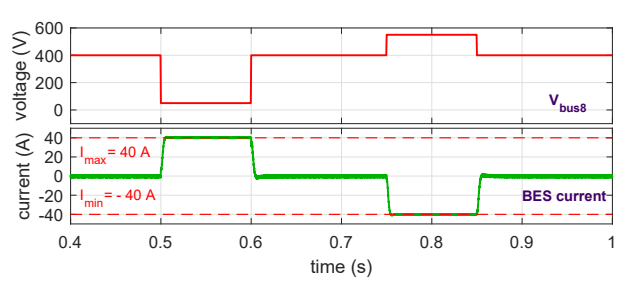


Fig. 16: Current limiting feature of the proposed controller.

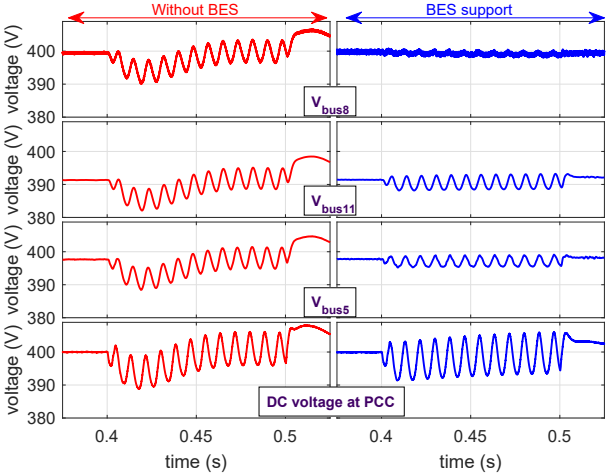


Fig. 17: Time response of the system during L-G fault on phase A.

oscillations. With the BES, the voltage oscillations near the point of connection of the BES are significantly reduced.

5) SOC Control Test: To show the concept of SOC control within a short simulation interval, a small battery (Q=0.1 Ah) is considered. Figure 18 shows the closed loop poles of the SOC loop when q_1 and q_2 are subsequently increased between $10^{-7} \rightarrow 10^{-1.75}$ and $10^1 \rightarrow 10^{0.75}$, respectively. The control gains are $k_{1\rm soc}=0.1334$ and $k_{2\rm soc}=-10.08$ with the closed loop poles at $-0.014 \pm j0.013$. The SOC limit parameters are $SoC_{\rm set}=0.5$, $SoC_{\rm a}=0.3$, $SoC_{\rm b}=0.7$, $SoC_{\rm min}=0.2$, $SoC_{\rm max}=0.8$, and $\gamma=2$. Figure 19 shows the response of the BES system to the rise in PV power. Since the bus voltage($v_{\rm g}$) is higher than the set value of 400 V, the BES provides static support by absorbing power from the system that results in the rise of SOC. The reference current

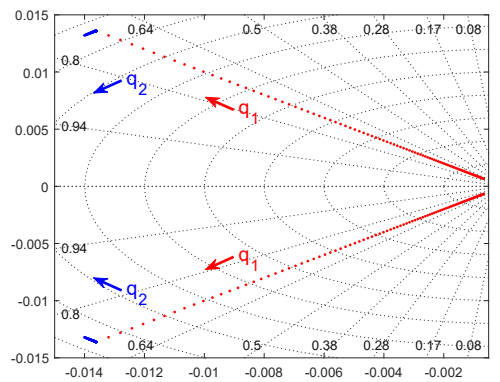


Fig. 18: Design of SOC control gains of BES converter.

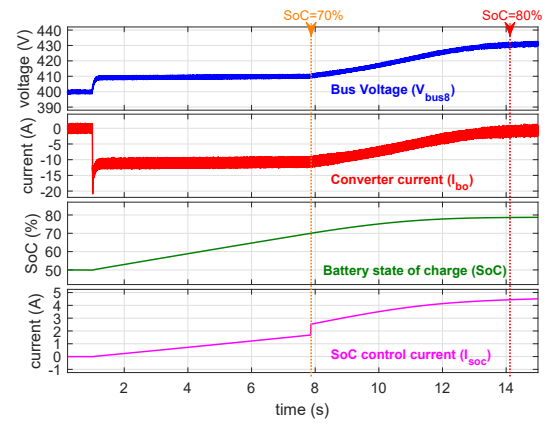


Fig. 19: SOC control response of the proposed BES system.

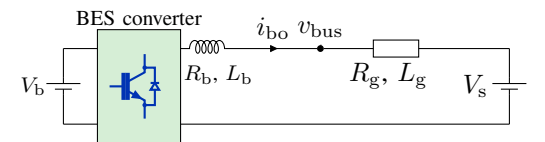


Fig. 20: Schematic circuit diagram for comparison part.

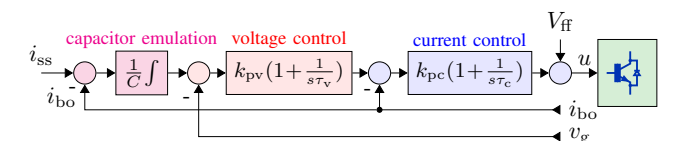


Fig. 21: Control structure of a conventional approach.

for SOC control $(I_{\rm soc})$ also rises indicating that the battery should discharge to drive the SOC back to its nominal value. When the SOC reaches the boundary condition of 70%, the controller starts disabling the static support and at the upper limit of 80%, the static support is completely disabled.

6) Comparison with Conventional Approach: In the conventional approaches, shown in Fig. 21, the current and voltage controls are designed separately and the feedback branch via k_3 is absent [30], [31]. This requires a significantly slower voltage loop to avoid interference with the current loop. During the weak grid conditions and especially at small C, this results in poor performance.

Figure 20 shows the circuit diagram of a study system to compare the performances of the proposed method with the conventional approach. The BES at 600 V is connected to a dc bus with a nominal voltage of 400 V through a bi-directional

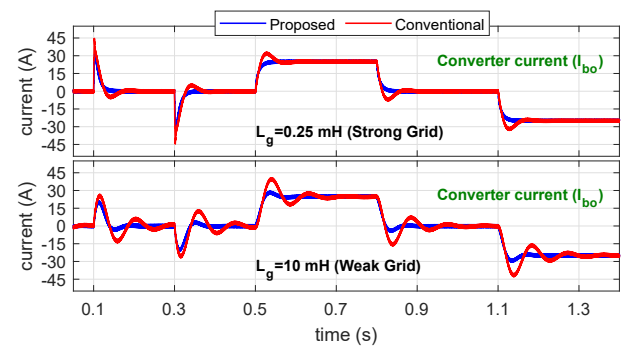


Fig. 22: Responses of proposed and conventional approaches to voltage disturbances and power commands in strong and weak grid conditions.

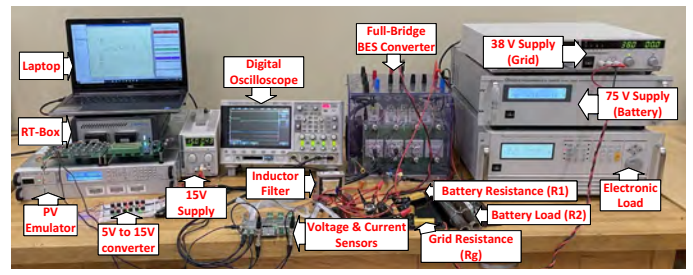


Fig. 23: Experimental setup.

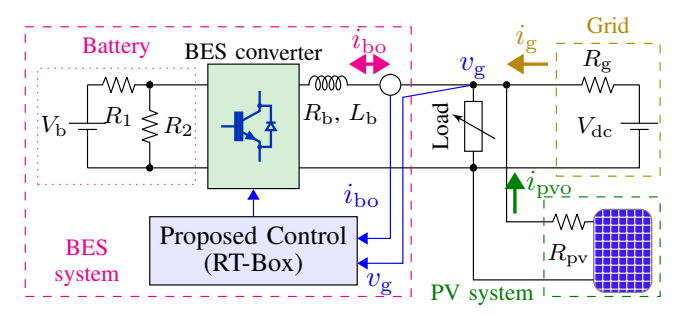


Fig. 24: Schematic circuit diagram of the experimental setup.

converter. The converter has an output filter with inductance $L_{\rm b}=2.5$ mH and resistance $R_{\rm b}=50$ m Ω . It is desired to emulate a virtual capacitance (C) of 10 mF with R_v =0.8. The grid impedance has resistance $(R_{\rm g})$ of 5 m Ω and inductance (L_g) of 0.25 mH for strong grid and 10 mH for weak grid. The feedback gains in the proposed approach are k_1 =-3162, k_2 =5.4, and k_3 =-12.15 with closed loop poles at $-1007\pm j941$, -166. In the conventional approach, the current and voltage controllers are designed separately with current loop several times faster than the voltage loop. In this study, the current control parameters are $k_{\rm pc}=4.97,\, \tau_{\rm c}=0.0011$ such that the poles are at $-1004 \pm j73$ to match with the fast poles of the proposed system. The voltage control parameters are $k_{\rm pv} =$ 0.948, $\tau_{\rm v}=0.0133$ such that the poles are at $-95\pm j73$ to make them 10 times slower than the current loop. The voltage loop poles are near the third pole of the proposed current controller.

Voltage disturbances and power commands are applied to observe the performance of the proposed controller against the conventional approach in strong and weak grid situations. At t=0.1 s, the bus voltage drops from 400 V to 360 V (10%)

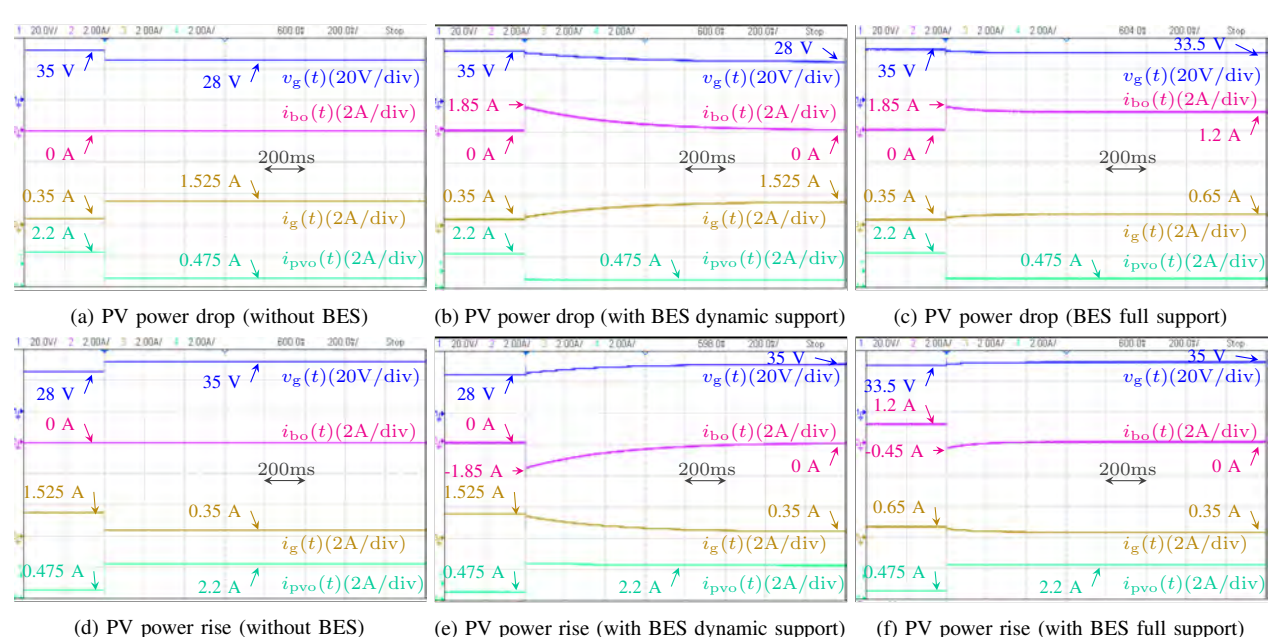


Fig. 25: Responses of the system to the PV disturbances in experimental setup.

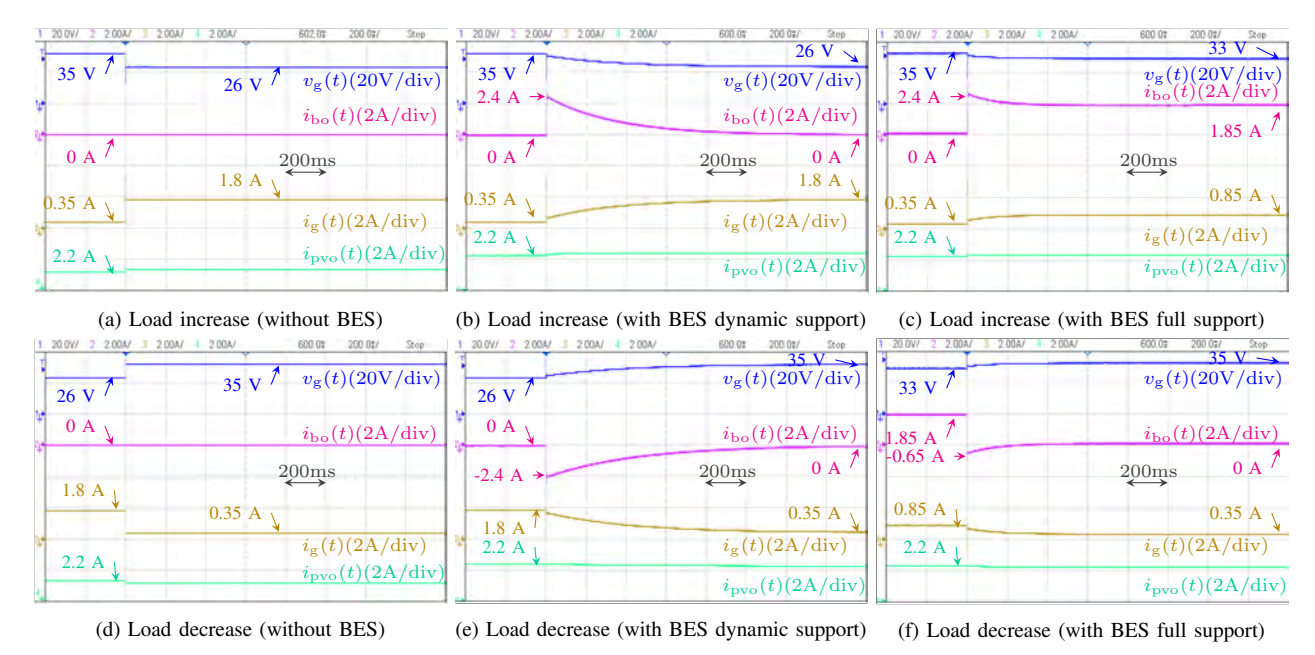


Fig. 26: Responses of the system to the load disturbances in experimental setup.

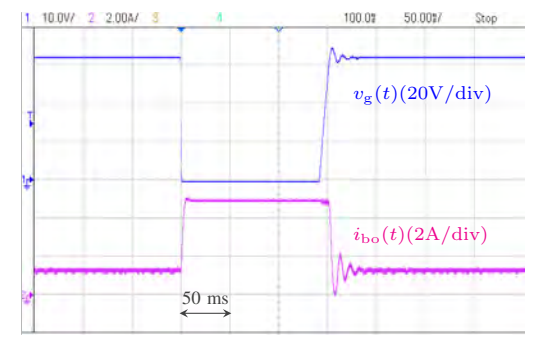


Fig. 27: Current limiting feature of the proposed controller

drop) and rises back to 400 V at t=0.3 s. The step power commands are applied by setting $P_{\rm set}$ at 10 kW, 0 kW and -10 kW at t=0.5 s, t=0.75 s, and t=1.1 s, respectively. For this study, the static support and SOC control are disabled. Figure 22 shows the converter current in response to the voltage disturbances and power commands. It can be clearly observed that both the proposed and conventional approaches have similar level of performance during the strong grid situation. However, the conventional one suffers from poor damping due to interaction of the voltage loop with the current loop in weak grid situations.

V. EXPERIMENTAL RESULTS

A. Experimental Setup

Figure 23 shows a photograph of the laboratory setup, and its circuit diagram is shown in Fig. 24. It consists of an Agilient E4360A PV emulator that operates at its maximum power point, a dc voltage source at $V_{\rm dc}$ =38 V behind a resistance ($R_{\rm g}$) of 6 Ω , and a Chroma programmable electronic load 63802. The load resistance is set to 12.73 Ω and the set voltage at the PCC ($V_{\rm g}$) is 35.0 V.

A BES system with the proposed controller (shown in Fig. 1) is interfaced at the PCC. A power supply at the voltage $V_{\rm b} = 75.0 \text{ V}$ with series resistance (R_1) of 3.0 Ω and load (R_2) of 50.0 Ω acts as the battery. It uses a fullbridge converter from Semikron and unipolar PWM at the switching frequency of 5 kHz. The converter output filter inductance (L_b) is 10 mH and its parasitic resistance (R_b) is 0.4 Ω . The emulated capacitance (C) is 100 mF and the virtual resistance (R_v) is 0.5 Ω . The current control gains are designed based on method discussed in Section III-4: with $q_1 = 10^{7.5}$, $q_2 = 10^{1.5}$, and $q_3 = 10^2$, the control gains are $k_1 = -5623.0$, $k_2 = 11.8$, and $k_3 = -24.0$, and the closed loop poles are located at $-600 \pm j449$ and -20. The droop gain $(K_{\rm v})$ is set at 18.75 meaning that the BES supplies/absorbs 18.75 W per a unit of voltage offset. The maximum (I_{max}) and the minimum (I_{\min}) current limits are set at 5 A and -5 A. The controller is implemented in RT-Box from Plexim [40].

B. Experimental Results

- 1) Case I: PV Disturbances: Figures 25(a)-(c) show the responses when the PV current (i_{pvo}) is decreased from 2.2 A to 0.475 A. Without the BES support, this drop in PV power causes a sudden sag in the PCC voltage (v_g) from 35.0 V to 28.0 V and a sudden rise in the grid current (i_g) from 0.35 A to 1.525 A. With the BES dynamic support, the BES provides inertia by quick supply of current (i_{bo}) with peak of 1.85 A that prevents sudden drop in the voltage similar to an actual capacitor of 100 mF. When the static support is enabled, the BES continues to supply current (i_{bo}) of 1.20 A that holds the voltage at 33.5 V. Similarly, Figures 25(d)-(f) show the responses when the PV current (i_{pvo}) is increased from 0.475 A to 2.2 A. Same conclusions are drawn.
- 2) Case II: Load Disturbances: Figures 26(a)-(c) show the response when the load resistance is decreased from 12.73 Ω to 6.0 Ω . This results in a sudden drop in the voltage at PCC $(v_{\rm g})$ from 35.0 V to 26.0 V and a rise in the grid current $(i_{\rm g})$ to 1.8 A from 0.35 A. With the dynamic support, the BES provides inertia by injecting current with the peak of 2.4 A, and it is slowly reduced to zero. With the static support, the BES continuous to supply current $(i_{\rm bo})$ of 1.85 A that holds the voltage at 33.0 V. Similarly, Figures 26(d)-(f) show the response when the load resistance is increased from 6.0 Ω to 12.73 Ω .
- 3) Case III: Current Limiting: Figure 27 shows the response of the BES when the voltage at the PCC suddenly drops from 34 V to 0.0 V due to short-circuit incident. The current is successfully limited at the pre-specified value of 5.0 A. The fault is cleared at 150 ms and the BES returns to its

normal operation. When the fault is cleared, there are voltage overshoots where the BES responds with the oscillating current to suppress these voltage overshoots.

The experimental results confirm the operation of the proposed system at low voltage/power. Since the system is linear, the scalability at high voltage/power applications is valid.

VI. CONCLUSION

The battery energy storage (BES) systems are being increasingly adopted and their full integration is crucial. This paper presents a local controller for a BES system with the following capabilities. 1) The BES is autonomous and not dependent on a co-located renewable source. 2) It provides dynamic and static grid supports. 3) It provides converter current limiting. 4) It maintains the state-of-charge (SOC) of the battery. 5) It adjusts the level of static support according to the SOC level. 6) Its control system is robust/optimal and exhibits improved responses compared with conventional approaches. Investigating conditions other than those of this paper, and the field testing of the controller are future works.

VII. ACKNOWLEDGEMENT

The authors acknowledge with appreciation the financial support provided by the United States' National Science Foundations (NSF), under award numbers 1808368 and 1902791.

REFERENCES

- [1] "Sunshot 2030," https://www.energy.gov/eere/solar/sunshot-2030.
 [2] IEA, "World energy outlook 2020," https://www.iea.org/reports/world-
- energy-outlook-2020, 2020, accessed: 2020-12-06.
- [3] B. A. Mather, S. Shah, B. L. Norris, J. H. Dise, L. Yu, D. Paradis, F. Katiraei, R. Seguin, D. Costyk, J. Woyak et al., "NREL/SCE high penetration PV integration project: FY13 annual report," National Renewable Energy Lab.(NREL), Golden, CO (United States), Tech. Rep., 2014.
- [4] J. Hu, Z. Li, J. Zhu, and J. M. Guerrero, "Voltage stabilization: A critical step toward high photovoltaic penetration," *IEEE Industrial Electronics Magazine*, vol. 13, no. 2, pp. 17–30, 2019.
- [5] B. Kroposki, B. Johnson, Y. Zhang, V. Gevorgian, P. Denholm, B.-M. Hodge, and B. Hannegan, "Achieving a 100% renewable grid: Operating electric power systems with extremely high levels of variable renewable energy," *IEEE Power and energy magazine*, vol. 15, no. 2, pp. 61–73, 2017
- [6] "IEEE standard for interconnection and interoperability of distributed energy resources with associated electric power systems interfaces," *IEEE Std* 1547-2018, pp. 1–138, April 2018.
- [7] V. Henze, "Battery pack prices fall as market ramps up with market average at \$156/kwh in 2019," *BloombergNEF*, 2019.
- [8] B. T. Patterson, "Dc, come home: Dc microgrids and the birth of the "enernet"," *IEEE Power and Energy Magazine*, vol. 10, no. 6, pp. 60–69, 2012.
- [9] N. Kirby, "Current trends in dc: Voltage-source converters," *IEEE Power and Energy Magazine*, vol. 17, no. 3, pp. 32–37, May 2019.
- [10] G. Melath, S. Rangarajan, and V. Agarwal, "A novel control scheme for enhancing the transient performance of an islanded hybrid ac-dc microgrid," *IEEE Transactions on Power Electronics*, vol. 34, no. 10, pp. 9644–9654, 2019.
- [11] J. Wang, K. G. Sun, D. Zhou, and Y. R. Li, "Virtual SVPWM based flexible power control for dual-dc-port dc-ac converters in PV-battery hybrid systems," *IEEE Transactions on Power Electronics*, 2021.
- [12] E. Pritchard and D. C. Gregory, "The dc revolution," *IEEE Electrification Magazine*, vol. 4, no. 2, pp. 4–9, 2016.
- [13] M. Nasir, H. A. Khan, N. A. Zaffar, J. C. Vasquez, and J. M. Guerrero, "Scalable solar dc micrigrids: On the path to revolutionizing the electrification architecture of developing communities," *IEEE Electrification Magazine*, vol. 6, no. 4, pp. 63–72, 2018.

- [14] A. Chub, D. Vinnikov, O. Korkh, M. Malinowski, and S. Kouro, "Ultrawide voltage gain range microconverter for integration of silicon and thin-film photovoltaic modules in dc microgrids," *IEEE Transactions on Power Electronics*, 2021.
- [15] O. Gagrica, P. H. Nguyen, W. L. Kling, and T. Uhl, "Microinverter curtailment strategy for increasing photovoltaic penetration in lowvoltage networks," *IEEE Transactions on Sustainable Energy*, vol. 6, no. 2, pp. 369–379, 2015.
- [16] A. Sangwongwanich, Y. Yang, and F. Blaabjerg, "A cost-effective power ramp-rate control strategy for single-phase two-stage grid-connected photovoltaic systems," in *IEEE Energy Conversion Congress and Ex*position (ECCE), 2016, pp. 1–7.
- [17] N. Kakimoto, H. Satoh, S. Takayama, and K. Nakamura, "Ramp-rate control of photovoltaic generator with electric double-layer capacitor," *IEEE Transactions on Energy Conversion*, vol. 24, no. 2, pp. 465–473, 2009
- [18] X. Li, D. Hui, and X. Lai, "Battery energy storage station (BESS)-based smoothing control of photovoltaic (PV) and wind power generation fluctuations," *IEEE Transactions on Sustainable Energy*, vol. 4, no. 2, pp. 464–473, 2013.
- [19] M. Alam, K. Muttaqi, and D. Sutanto, "A novel approach for ramp-rate control of solar PV using energy storage to mitigate output fluctuations caused by cloud passing," *IEEE Transactions on Energy Conversion*, vol. 29, no. 2, pp. 507–518, 2014.
- [20] R. Sharma and M. Karimi-Ghartemani, "Addressing abrupt PV disturbances, and mitigating net load profile's ramp and peak demands, using distributed storage devices," *Energies*, vol. 13, no. 5, p. 1024, 2020.
- [21] P. J. dos Santos Neto, T. A. dos Santos Barros, J. P. C. Silveira, E. Ruppert Filho, J. C. Vasquez, and J. M. Guerrero, "Power management strategy based on virtual inertia for dc microgrids," *IEEE Transactions on Power Electronics*, vol. 35, no. 11, pp. 12472–12485, 2020.
- [22] H.-P. Beck and R. Hesse, "Virtual synchronous machine," in 9th International Conference on Electrical Power Quality and Utilisation. IEEE, 2007, pp. 1–6.
- [23] M. Karimi-Ghartemani, S. A. Khajehoddin, P. Piya, and M. Ebrahimi, "Universal controller for three-phase inverters in a microgrid," *IEEE Journal of Emerging and Selected Topics in Power Electronics*, vol. 4, no. 4, pp. 1342–1353, 2016.
- [24] J. Fang, P. Lin, H. Li, Y. Yang, and Y. Tang, "An improved virtual inertia control for three-phase voltage source converters connected to a weak grid," *IEEE Transactions on Power Electronics*, vol. 34, no. 9, pp. 8660–8670, 2018.
- [25] T. Shucheng, D. Ge, Z. Hui, Z. Na, and X. Xi, "Virtual dc machine control strategy of energy storage converter in dc microgrid," in *Electrical Power and Energy Conference (EPEC)*. IEEE, 2016, pp. 1–5.
- [26] E. Unamuno, J. Paniagua, and J. A. Barrena, "Unified virtual inertia for ac and dc microgrids: And the role of interlinking converters," *IEEE Electrification Magazine*, vol. 7, no. 4, pp. 56–68, 2019.
- [27] W. Wu, Y. Chen, A. Luo, L. Zhou, X. Zhou, L. Yang, Y. Dong, and J. M. Guerrero, "A virtual inertia control strategy for dc microgrids analogized with virtual synchronous machines," *IEEE Transactions on Industrial Electronics*, vol. 64, no. 7, pp. 6005–6016, 2016.
- [28] Y. Wang, C. Wang, L. Xu, J. Meng, and Y. Hei, "Adjustable inertial response from the converter with adaptive droop control in dc grids," *IEEE Transactions on Smart Grid*, vol. 10, no. 3, pp. 3198–3209, 2018.
- [29] N. Zhi, K. Ding, L. Du, and H. Zhang, "An SOC-based virtual dc machine control for distributed storage systems in dc microgrids," *IEEE Transactions on Energy Conversion*, vol. 35, no. 3, pp. 1411–1420, 2020.
- [30] E. Unamuno and J. A. Barrena, "Design and small-signal stability analysis of a virtual-capacitor control for dc microgrids," in 19th European Conference on Power Electronics and Applications (EPE'17 ECCE Europe), 2017, pp. P.1–P.10.
- [31] X. Zhu, F. Meng, Z. Xie, and Y. Yue, "An inertia and damping control method of dc-dc converter in dc microgrids," *IEEE Transactions on Energy Conversion*, vol. 35, no. 2, pp. 799–807, 2019.
- [32] Y. Yang, C. Li, J. Xu, F. Blaabjerg, and T. Dragicevic, "Virtual inertia control strategy for improving damping performance of dc microgrid with negative feedback effect," *IEEE Journal of Emerging and Selected Topics in Power Electronics*, 2020.
- [33] M. Karimi-Ghartemani, S. A. Khajehoddin, P. Jain, and A. Bakhshai, "Linear quadratic output tracking and disturbance rejection," *International Journal of control*, vol. 84, no. 8, pp. 1442–1449, 2011.
- [34] T. Qunais, R. Sharma, M. Karimi-Ghartemani, S. Silwal, and S. A. Khajehoddin, "Application of battery storage system to improve transient responses in a distribution grid," in 28th International Symposium on Industrial Electronics (ISIE). IEEE, 2019, pp. 52–57.

- [35] I. Serban and C. Marinescu, "Control strategy of three-phase battery energy storage systems for frequency support in microgrids and with uninterrupted supply of local loads," *IEEE Transactions on power* electronics, vol. 29, no. 9, pp. 5010–5020, 2013.
- [36] N. A. Ashtiani, S. A. Khajehoddin, and M. Karimi-Ghartemani, "Optimal design of nested current and voltage loops in grid-connected inverters," in *Applied Power Electronics Conference and Exposition (APEC)*. IEEE, 2020, pp. 2397–2402.
- [37] M. A. G. De Brito, L. Galotto, L. P. Sampaio, G. d. A. e Melo, and C. A. Canesin, "Evaluation of the main mppt techniques for photovoltaic applications," *IEEE transactions on industrial electronics*, vol. 60, no. 3, pp. 1156–1167, 2013.
- [38] S. Silwal, M. Karimi-Ghartemani, R. Sharma, and H. Karimi, "Impact of feed-forward and decoupling terms on stability of grid-connected inverters," in 28th International Symposium on Industrial Electronics (ISIE). IEEE, 2019, pp. 2641–2646.
- [39] M. Karimi-Ghartemani, Enhanced phase-locked loop structures for power and energy applications. John Wiley & Sons, 2014.
- [40] "RT Box," "https://www.plexim.com/products/rt_box".



Roshan Sharma (S'17) received his B.E. degree in Electrical Engineering from Institute of Engineering, Tribhuvan University, Nepal in 2013, and the Ph.D. degree in Electrical and Computer Engineering from Mississippi State University, Mississippi State, MS, USA, in 2021.

He is currently working in Smart Grid and Emerging Technology group at Commonwealth Edison (ComEd) Company, Chicago, IL, USA. His research interest include control and integration of distributed and renewable energy resources, microgrids, power

system dynamics, modeling and control.



Ali Zakerian (S'21) received the B.Sc. and M.Sc. degrees from Urmia University, Urmia, Iran, in 2013 and 2015, respectively, both in electrical power engineering. He is currently working toward the Ph.D. degree in electrical and computer engineering at Mississippi State University, Mississippi State, MS, USA.

His research interests include control and integration of renewable energy resources, modeling, design, analysis, and control of power electronics, distributed energy resources and microgrids.



Masoud Karimi-Ghartemani (M'01-SM'09) received his Ph.D. in Electrical and Computer Engineering from University of Toronto in 2004. He was a faculty member with Electrical Engineering Department at Sharif University of Technology, Tehran, during 2005-2008 and a member of ePOWER laboratory at Queen's University, Canada, during 2008-2011. Since 2012, he has been with the Department of Electrical and Computer Engineering at Mississippi State University (MSU), USA, where he is currently a Professor. His general research area

is power system analysis, stability and control. His particular research interest is in the integration of distributed and renewable energy systems. He works on modeling, control, and operation of distributed energy systems at high penetration level. He is the winner of 2020 faculty research award at MSU's Bagley College of Engineering. Dr. Karimi is an Associate Editor of IEEE Transactions on Industrial Electronics and IEEE Transactions on Sustainable Energy.